Universities Council on Water Resources
Journal of Contemporary Water Research & Education
Issue 160, Pages 132-143, April 2017

2D-Fe_3O_4 Nanosheets for Effective Arsenic Removal

Hongxi Luo[1], Fangwei Cheng[1], Weiming Hu[2], Jinpeng Wang[1], Shuting Xiang[1], and *Maria Fidalgo de Cortalezzi[2]

[1]*Department of Chemical Engineering, University of Missouri, Columbia, MO, USA*
[2]*Department of Civil & Environmental Engineering, University of Missouri, Columbia, MO, USA*
**Corresponding author*

Abstract: Fe_3O_4 adsorbent with 2D structures was synthesized via solvothermal method and its application in arsenic removal was investigated. Isotherms were generated at pH=4.7 and 7.6 and the results were best fitted by the Freundlich isotherm model; good As(V) adsorption capacity was achieved for the Fe_3O_4 adsorbent at both pH values. Furthermore, pH effects were evaluated; the optimal pH value for adsorption was 8.27 with the adsorption capacity and the removal efficiency being 18.55 mg/g and 93.69%, respectively. Based on the measurements of the zeta potential and particle size of the adsorbent, we proposed that the overall pH dependence was a result of the combined effects of the zeta potential, particle size of the adsorbent, and existing form of As(V). From kinetics studies, the As(V) adsorption by Fe_3O_4 adsorbent followed the pseudo-second-order model and could be described by a two stage mechanism. When initial As(V) concentration was 1 ppm, 73% of the As(V) was adsorbed within the first 2.5 minutes and an overall removal efficiency of 82.5% was achieved in 2 hours. Increased removal efficiency is expected at higher adsorbent loading, thus allowing the post-treatment water to meet drinking water quality standards.

Keywords: *adsorption, Fe_3O_4 adsorbent, arsenic removal, 2D structure, water treatment*

Arsenic, a toxic element commonly found in waters and soils, has become a huge threat to public health in the recent years (Hughes 2002; Smedley and Kinniburgh 2002). Both organic and inorganic forms of arsenic exist in the environment, while the latter is of higher toxicity and frequently found in groundwater (Styblo et al. 2000; Mandal and Suzuki 2002). Inorganic arsenic typically has two oxidation states, As(III) and As(V), and its presence in groundwater is a severe environmental problem (Hughes 2002; Mandal and Suzuki 2002; Hung et al. 2004). It is believed that long term exposure to arsenic contaminated water increases the risk of skin, lung, kidney, and liver cancer as well as skin pigmentation and neurological disorders (Mandal and Suzuki 2002). In 1993, the World Health Organization (WHO) revised its guideline value for arsenic in potable water, lowering it from 50 µg/L to 10 µg/L, to limit the adverse effects of arsenic contamination (Jain and Singh 2012). However, some countries, like Bangladesh, maintain the earlier WHO standard even though research proves that exposure to arsenic at low levels (<10 ppb) increases the risk of skin cancer (Mandal and Suzuki 2002). In the typical range of groundwater pH (6.0-8.5) (Heath 1984), As(III) mainly exists as the neutral molecule (H_3AsO_3) while As(V) exists as anions ($H_2AsO_4^-$ and $HAsO_4^{2-}$). In the absence of electrostatic interactions, the adsorption of As(III) is limited by the available surface sites of the adsorbent. The adsorption of As(V) is usually more favorable under the same conditions so the removal of arsenic as As(V) is more effective (Yazdani et al. 2016). Hence, this study will focus on As(V); furthermore, As(III) can be treated following a pretreatment (oxidation) step.

During the past decades, studies have focused on the development of effective arsenic removal techniques such as membrane separation, coagulation/precipitation, ion exchange, and adsorption (Hung et al. 2004; Litter et al. 2010).

Adsorption is a competitive method due to its simplicity, low-cost, and good adsorbent reusability (Mohan and Pittman 2007; Cheng et al. 2016). Several categories of adsorbents including activated carbon (Litter et al. 2010; Amano et al. 2014), activated alumina (Guan et al. 2009; Litter et al. 2010), and iron-oxide-based adsorbents (Dixit and Hering 2003; Giles et al. 2011) have been studied intensely and applied in arsenic removal. In particular, iron-oxide-based adsorbents such as amorphous hydrous ferric oxide (FeO-OH), goethite (α-FeO-OH), hematite (α-Fe_2O_3), and magnetite (Fe_3O_4) are very effective due to the high affinity of iron towards arsenic (Litter et al. 2010). The magnetic response feature of Fe_3O_4 makes it possible for adsorbent separation by simply applying an external magnetic field after adsorption (Yavuz et al. 2006), therefore great efforts have been devoted to design Fe_3O_4 (Shipley et al. 2009) and its composites (Chang et al. 2012) with special structures to achieve effective arsenic removal. Recently, the synthesis of 2D ultrathin nanosheet for several metal oxides, including Fe_3O_4, was reported by Sun et al. (2014). Compared with conventional metal oxide nanoparticles, the unique 2D structures offered significantly higher specific surface areas (Sun et al. 2014), which is beneficial in the adsorption processes. Moreover, such structure has the potential to reduce the mass transfer resistance aroused from the tortuosity factors, resulting in improved kinetics. These properties led us to investigate its performance in arsenic removal.

In this work, we report the application of 2D Fe_3O_4 nanosheets in arsenic removal. The main objectives of the present work are (i) to examine the adsorption behavior of the adsorbent at different initial As(V) concentrations, (ii) to clarify the effects of pH on As(V) removal, and (iii) to investigate the adsorption kinetics of the adsorbent. Isotherms were generated at pH=4.7 and pH=7.6 and their results were fitted with Freundlich and Langmuir isotherm models. Single batch adsorption tests were carried out at different pH values ranging from 2 to 12. The zeta potential and particle size of the adsorbent material were also evaluated in the same interval for a better understanding of the influence of pH on adsorption. In addition, the adsorption kinetics was investigated. In general, 2D Fe_3O_4 nanosheets possessed good adsorption capacity and fast adsorption kinetics and therefore constitute a promising candidate material for effective arsenic removal.

Materials

Pluronic P123 (PEO_{20}-PPO_{70}-PEO_{20}, Sigma-Aldrich), absolute ethanol (C_2H_5OH, Sigma-Aldrich), iron nitrate nonahydrate ($Fe(NO_3)_3 \cdot 9H_2O$, Sigma-Aldrich), hexamethylenetetramine (HMTA, $C_6H_{12}N_4$, Sigma-Aldrich), ethylene glycol (EG, $(CH_2OH)_2$, Sigma-Aldrich), and DI water (H_2O) were used in the iron oxide synthesis. Dibasic sodium arsenate heptahydrate ($Na_2HAsO_4 \cdot 7H_2O$, Sigma-Aldrich), MES ($C_6H_{13}NO_4S \cdot H_2O$, Sigma-Aldrich), and DI water were used to prepare arsenic stock solution for adsorption studies. Hydrochloric acid (HCl, Sigma-Aldrich) and sodium hydroxide (NaOH, Sigma-Aldrich) were used for pH adjustments. Sodium nitrate ($NaNO_3$, Sigma-Aldrich) was used to control the ionic strength of the arsenic solution. All chemicals were of analytical reagent (AR) and used directly without further purification.

Preparation of 2D Fe_3O_4 Adsorbent

2D Fe_3O_4 adsorbent was synthesized via the route reported by Sun et al. (2014). In a typical experiment, 1.33 g P123 was added into 20 g absolute ethanol and the mixture was stirred for 15 minutes to form a homogeneous solution. 1.33 g iron nitrate nonahydrate and 0.467 g HMTA were then added into the ethanolic solution and the solution was stirred for another 15 minutes. After that, 86.7 mL EG was added and the solution was stirred for 30 minutes. The transparent dark orange precursor solution was obtained and allowed to age for two days. After two days, the precursor solution was transferred to a 200 mL autoclave with Teflon liner for solvothermal reaction. The autoclave was heated from room temperature (25 °C) to 150 °C at a rate of 5 °C/min and held at 150 °C for 15 hours. The precipitate was washed with absolute ethanol and DI water by three cycles of centrifugation (6000 rpm for 15 min at room temperature) and resuspension, dried at 80 °C overnight and sintered at 400 °C (heating rate =10 °C/min) for 10 hours in stagnant air to form the dark magnetic powder.

Material Characterizations

The crystal structures of the as-synthesized Fe_3O_4 adsorbent were characterized by X-ray diffraction in a Rigaku Ultima IV X-ray diffractometer using Cu Kα radiation (tension = 40 kV, current = 20 mA). Transmission electron microscopy (Tecnai F30 Twin transmission electron microscope (FEI)) was applied to investigate the structures and morphologies of the sample. The specific surface areas (calculated with BET method) of the Fe_3O_4 adsorbent were measured by isothermal nitrogen adsorption-desorption analysis (Beckman Coulter SA3100). The zeta potential and particle size of Fe_3O_4 adsorbent were measured by Dynamic Light Scattering (DLS) (Nanosizer ZS, Malvern).

Arsenic Adsorption Studies

Adsorption Isotherms

To investigate the adsorption performances of Fe_3O_4 adsorbent towards arsenate, adsorption isotherms were generated and studied. A determined amount of $Na_2HAsO_4{\cdot}7H_2O$ was dissolved in 1 L DI water to obtain 20 ppm As(V) stock solution. The solution was buffered by adding 9.5 g MES and its ionic strength was controlled by adding 0.85 g $NaNO_3$ (10 mM). In a typical experiment, 100 mL of the As(V) stock solution prepared was taken and its pH value was adjusted to 4.7 by adding 1M HCl solution. The total volume of HCl added was small compared to that of the As(V) solution, so that dilution effects could be neglected. The solution was then divided and diluted with 10 mM $NaNO_3$ at same pH to nine different initial concentrations, namely 1 ppm, 2 ppm, 3 ppm, 5 ppm, 7.5 ppm, 10 ppm, 12.5 ppm, 16 ppm, and 20 ppm. Then, a mass of 10 mg of Fe_3O_4 adsorbent was added to a 20 mL glass vial containing 10 mL as-prepared solution at each concentration. The vials were sealed and shaken by a vertical rotational shaker (shaking rate=80 rpm) for 24 hours to reach equilibrium. Fe_3O_4 adsorbent was separated from each vial by membrane filtration (Millipore GSWP2500, pore size 0.22 μm) after adsorption tests and the residual arsenic concentration in each solution was analyzed by Graphite Furnace Atomic Absorption Spectroscopy (GFAAS) using a BUCK Scientific, Model 220-GF. Hence, the amount of arsenic adsorbed per mass of adsorbent (g As/g Fe_3O_4) was determined with the following equation:

$$\text{As adsorbed (g As/g } Fe_3O_4) = \frac{(C_0 - C_1) * V}{m_{ad}} \quad \text{(Eq. 1)}$$

where C_0 and C_1 represented the initial and final As concentrations, V was the volume of the solution, and m_{ad} was the mass of Fe_3O_4 applied.

Another isotherm at pH=7.6 was obtained following the same procedures but the pH of As(V) solution was adjusted by adding 1M NaOH solution rather than HCl solution.

pH Effects on Adsorption

The effects of pH on adsorption were studied by carrying out batch adsorption experiments at nine different pH values, ranging from 2 to 12. It should be noted that the As(V) solution used for pH effects studies was not buffered with MES, but its ionic strength was still controlled by adding 10 mM $NaNO_3$. The pH value was adjusted to the desired value using small volumes of 1M HCl/NaOH solution. In a typical experiment, 10 mg Fe_3O_4 adsorbent was dispersed in 10 mL 20 ppm As(V) solution in each 20 mL glass vial. These vials were sealed and shaken by a vertical rotational shaker (shaking rate=80 rpm) for 24 hours to reach equilibrium. After adsorption tests, the adsorbent was removed by filtration and the final As(V) concentrations were measured by GFAAS. Equilibrium pH values for each solution measured by pH meter were 2.30, 3.15, 3.95, 5.19, 7.30, 8.27, 9.07, and 11.65, respectively.

Adsorption Kinetics

Adsorption kinetics were studied around pH=8.3, an optimal value determined by the pH tests. Herein, 2 ppm As(V) stock solution was prepared and buffered with MES. Its pH value was adjusted to 8 using a small volume of 1M NaOH and its ionic strength was again controlled by 10 mM $NaNO_3$. Unlike the previous tests, 2 mg Fe_3O_4 adsorbent was first added to a 20 mL vial containing 5 mL solution with the same pH and ionic strength, but in the absence of arsenate. The mixture was then shaken for 30 minutes to guarantee full dispersion of the adsorbent particles. At t=0, 5 mL 2 ppm As(V) solution, prepared previously, was

added to the vial to start adsorption. The vial was shaken by a vertical rotational shaker (shaking rate=80 rpm) for a determined time period and the Fe_3O_4 adsorbent was separated from the solution by filtration immediately after sampling to prevent further adsorption. The tests were carried out for nine different time periods, namely 2.5 min, 5 min, 10 min, 15 min, 20 min, 30 min, 40 min, 60 min, and 120 min; the final As(V) concentrations were measured by GFAAS.

Results and Discussion

Characterizations of Fe_3O_4 Adsorbent

The crystal structures of Fe_3O_4 were investigated by XRD. A typical diffraction pattern with 2θ ranging from 20˚ to 70˚ is shown in Figure 1. Diffraction peaks at 30.38˚, 35.63˚, 43.48˚, 54.03˚, 57.45˚, and 62.92˚, corresponding to (220), (311), (400), (422), (511), and (440) planes of magnetite (JCPDS No. 75-0449), were found in the pattern, verifying the presence of Fe_3O_4 in the bulk phase (He et al. 2007; Fan et al. 2011). Meanwhile, the sharp peaks indicate the formation of good crystallinity in the sample. However, peaks labeled with red circles at 24.15˚, 33.25˚, 41.03˚, and 49.50˚, corresponding to (012), (104), (113), and (024) plane of hematite (JCPDS No. 79-1741), were also observed, demonstrating the existence of α-Fe_2O_3 (Xu et al. 2015). The Fe_2O_3 phase might arise from the partial oxidation of the Fe_3O_4 phase during the drying and calcination process. Rietveld refinement was performed to estimate the content of each phase. As shown in Figure 1 (b), the refined sample XRD pattern could be broken down into the refined patterns for pure magnetite and hematite, respectively. The estimated content of the Fe_3O_4 phase was 80.9% and that of the Fe_2O_3 phase was 19.1%, indicating that only a small portion of Fe_3O_4 was oxidized. Moreover, the XRD pattern in Figure 1 (a) was also compared with that obtained by Sun et al. (2016); all peaks with the same shapes were found at identical locations.

The morphology of as-synthesized Fe_3O_4 was characterized by TEM and typical images are presented in Figure 2, at three different magnifications. From Figure 2 (a) and (b), it can be observed that the as-synthesized Fe_3O_4

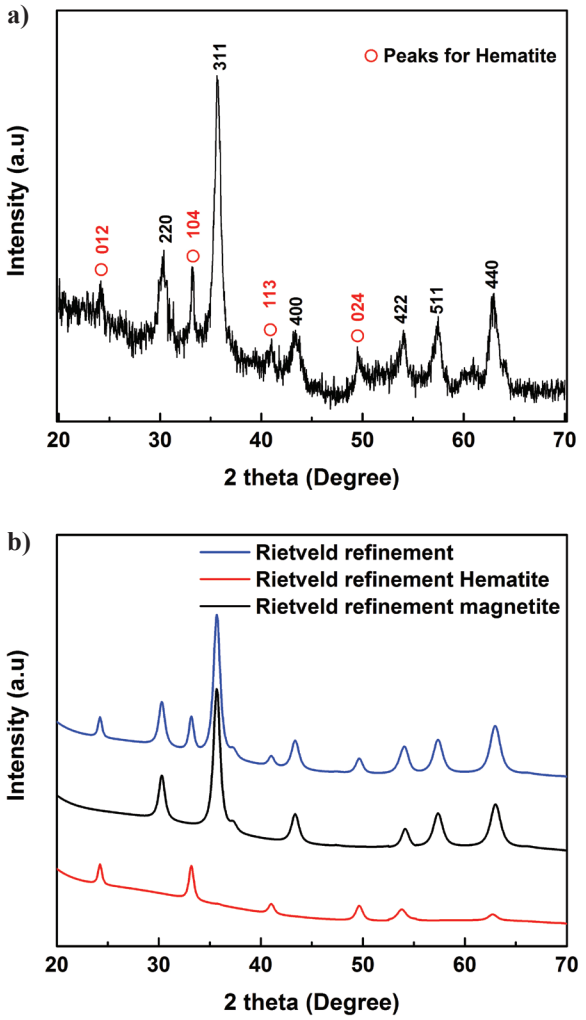

Figure 1. (a) Typical XRD pattern of as-synthesized Fe_3O_4 adsorbent. (b) Rietveld refinement of the obtained XRD pattern.

particles were mostly thin sheets, showing their 2D structure. It should also be noted that the particles did not exhibit uniformity, either in shape or size, and aggregation was observed, which can be explained from the high surface energy nature of 2D materials (Sun et al. 2016). Additionally, branched structures, with a thickness ranging from 5 nm to 20 nm, were found, as shown for example in Figure 2 (c). Such structures might be interpreted as stacks of several single layer sheets, which further verified the existence of the 2D structure in the Fe_3O_4 adsorbent fabricated. The BET specific surface area of the adsorbent was 94.07 m^2/g.

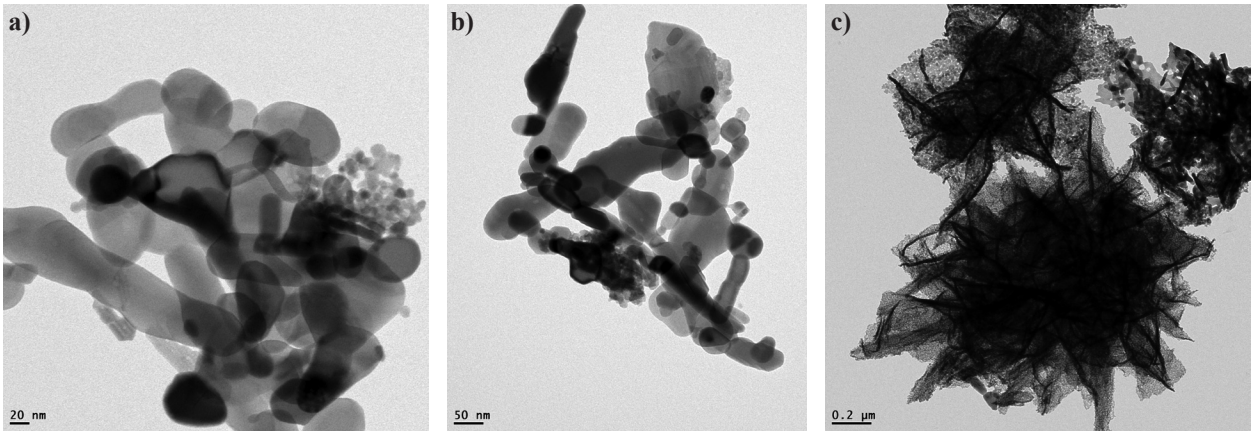

Figure 2. TEM images of as-synthesized Fe_3O_4 at different magnifications; Scale bar: (a) 20 nm, (b) 50 nm, and (c) 0.2 µm.

As(V) Adsorption Studies

Adsorption Isotherms

To investigate the As(V) adsorption capacity of Fe_3O_4 adsorbent, an adsorption isotherm at pH=4.7 was generated and the results are presented in Figure 3 (a). When the initial As(V) concentration was 20 ppm, the corresponding equilibrium adsorption capacity for Fe_3O_4 adsorbent was calculated to be 14.14 mg As/g adsorbent. For a better understanding of the adsorption behaviors, two commonly used adsorption models, the Freundlich (Borys and Grzywna 2016) and Langmuir (Ajay et al. 2014) isotherm models, were applied in data fitting.

The Freundlich isotherm model is presented by the following equation:

$$Q_e = K_f C_e^{\frac{1}{n}} \qquad \text{(Eq. 2)}$$

where Q_e and C_e represent the mass of As(V) adsorbed per mass of adsorbent (mg/g) and the equilibrium concentration of As(V) in solution (mg/L). The Freundlich isotherm constant K_f is an indication of the adsorption capacity (mg/g) of the adsorbent, and $1/n$ is the adsorption intensity (Borys and Grzywna 2016). The linear form of the Freundlich isotherm model is obtained by taking the logarithm of both sides and is given as:

$$\ln(Q_e) = \ln(K_f) + \tfrac{1}{n}\ln(C_e) \qquad \text{(Eq. 3)}$$

As shown in Figure 3 (b), the coefficient of determination R^2 is 0.99. The values for K_f and $1/n$ are 6.5562 mg/g and 0.4609, respectively. The data points are well fitted by the curve, demonstrating that the Freundlich isotherm model gives an excellent prediction for As(V) adsorption.

The Langmuir isotherm model is described as follows:

$$Q_e = \frac{Q_{max} K_l C_e}{1 + K_l C_e} \qquad \text{(Eq. 4)}$$

where the Langmuir isotherm constant K_l (L/mg) is related to the energy of adsorption, and Q_{max} is the maximum monolayer adsorption capacity (mg/g) (Ajay et al. 2014). The Langmuir isotherm model is linearized to the following form to determine Q_{max} and K_l:

$$\frac{1}{Q_e} = \frac{1}{Q_{max}} + \frac{1}{Q_{max} K_l C_e} \qquad \text{(Eq. 5)}$$

Clearly from Figure 3 (c), the data points do not match the linear fitting very well and the corresponding R^2 is 0.9607. The values for Q_{max} and K_l are 6.3591 mg/g and 11.6217 L/mg, respectively. Compared with the Freundlich model, the Langmuir model is less accurate in predicting the adsorption of As(V) in this case.

A second adsorption isotherm at pH=7.6 was also generated and the corresponding results are shown in Figure 4 (a). When the initial As(V) concentration was 20 ppm, the corresponding equilibrium adsorption capacity for Fe_3O_4

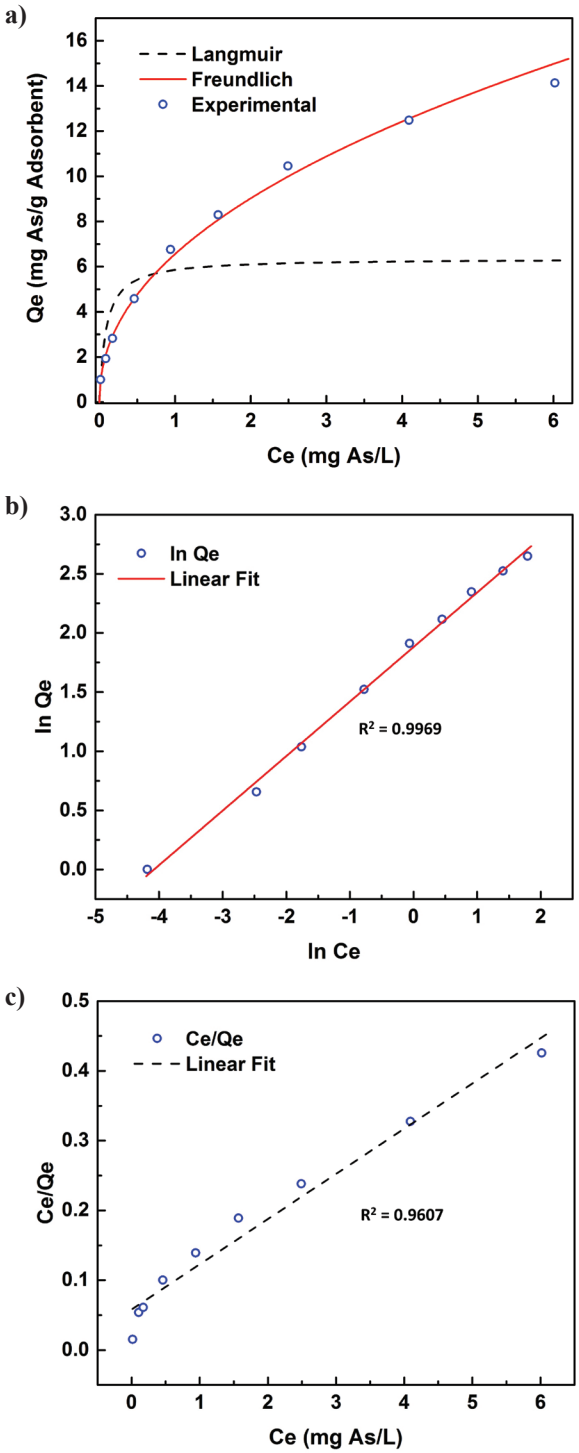

Figure 3. (a) Adsorption isotherm obtained at pH=4.7. Linear fitting curve for experimental data with (b) Freundlich model and (c) Langmuir model.

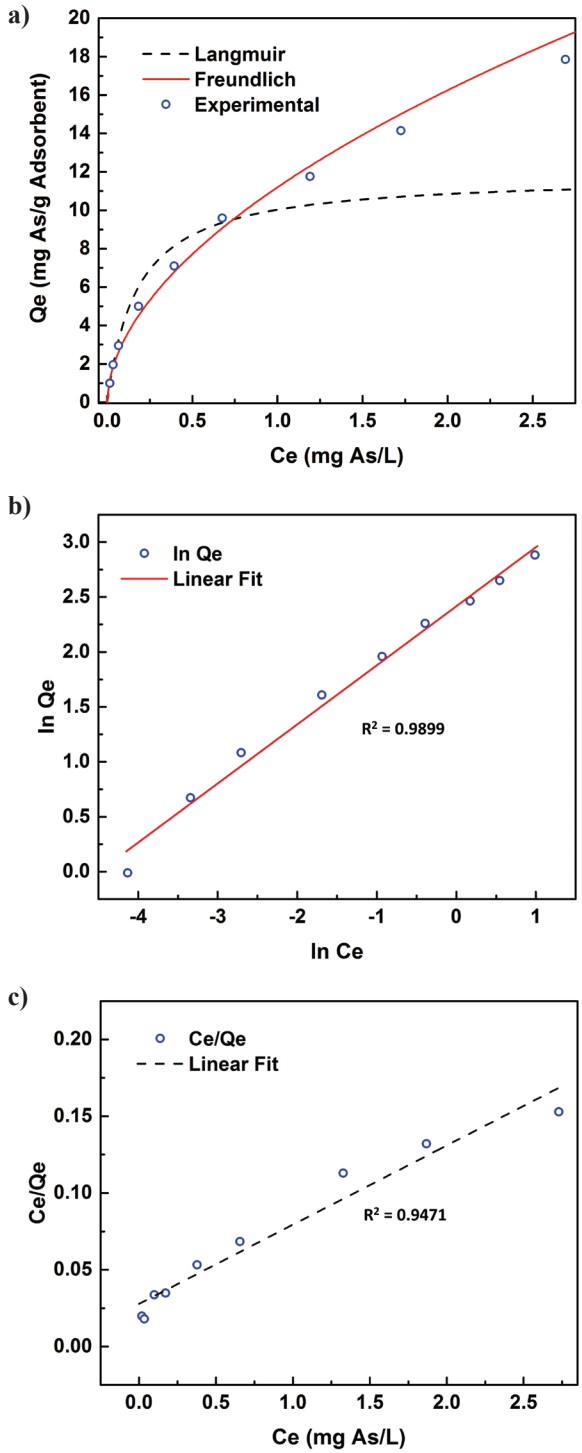

Figure 4. (a) Adsorption isotherm obtained at pH=7.6. Linear fitting curve for experimental data with (b) Freundlich model and (c) Langmuir model.

adsorbent was calculated to be 17.85 mg As/g adsorbent. Compared with the results obtained at pH=4.7, an increase in As(V) adsorption capacity was observed, indicating that As(V) adsorption became more favorable when pH was elevated from 4.7 to 7.6.

The data points were also fitted with the Freundlich and Langmuir isotherm models, as shown in Figure 4 (b) and (c). The Freundlich constants K_f and $1/n$ are 11.194 mg/g and 0.5376 while Q_{max} and K_l predicted from the Langmuir model are 11.8075 mg/g and 5.6323 L/mg. Similar to the results found at pH=4.7, the Freundlich model better fits the data points and gives a higher coefficient of determination R^2 than the Langmuir model (0.9889 vs. 0.9471). Therefore, As(V) adsorption by Fe_3O_4 adsorbent is better predicted by the Freundlich isotherm model at both pH values.

pH Effects on Adsorption

Adsorption of arsenate on iron oxides has been reported to be strongly pH dependent (Pierce and Moore 1980, 1982; Manning and Fendorf 1998) forming inner sphere complexes on the iron oxide surfaces (Hingston et al. 1971; Anderson and Malotky 1979; Lumsdon et al. 1984; Waychunas et al. 1993; Manceau 1995; Sun and Doner 1996, 1998; O'Reilly et al. 2001).

In metal oxides, specific adsorption occurs by the replacement of surface hydroxyl groups by the adsorbing species, (As_2O_3), (Cornell and Schwertmann 2003)

$$\equiv FeOH + As_2O_3^- \leftrightarrow \equiv FeOAs_2O_3 + OH^- \quad \text{(Eq. 6)}$$

$$\equiv (FeOH)_2 + As_2O_3^- \leftrightarrow \equiv FeOAs_2O_3^+ + 2OH^- \quad \text{(Eq. 7)}$$

representing the monodentate and bidentate mode or coordination respectively.

The relationship between pH values and As(V) adsorption capacity of Fe_3O_4 is revealed in Figure 5 (a). The As(V) adsorption capacity of Fe_3O_4 at each equilibrium pH (2.30, 3.15, 3.95, 5.19, 7.30, 8.27, 9.07, and 11.65) is 7.98, 9.68, 10.62, 14.38, 17.64, 18.55, 15.35, and 4.99 mg/g. It is clear that adsorption capacity of Fe_3O_4 increases with increasing pH when pH is lower than 8.27, and further increase in pH will result in reduction in the adsorption capacity. At either strong acidic (pH=2.30) or basic (pH=11.65) conditions, the adsorption capacity of Fe_3O_4 is remarkably lower compared with its maximum value at pH=8.27. Two opposing effects arise with increasing pH: 1) the relative concentration of the anionic form increases due to further deprotonation of $H_3As_2O_3$, and 2) a decrease in the number of surface ≡FeOH groups, producing a maximum in the adsorption envelope. A similar trend was observed for fluoride and silicate on goethite (Hingston et al. 1968), the peak corresponding to the pH of highest concentration of the complex at the surface. It should also be noted that the adsorption capacity obtained at pH=5.19 and pH=7.30 are in agreement with the results from isotherm studies in the previous section at adjacent pH values (4.70 and 7.6). Therefore, the performance of the as-prepared Fe_3O_4 adsorbent in arsenic removal is highly reliable.

The arsenic removal efficiency at each pH was calculated from adsorption capacity via Equation 1 and the results are presented in Figure 5 (b). Clearly, pH has the same influence on arsenic removal efficiency as it does on adsorption capacity. When pH is 8.27, the Fe_3O_4 adsorbent could realize its maximum As(V) removal efficiency of 93.69%. However, this value decreases significantly to 40.3% and 25.18% at pH=2.3 and 11.65, respectively. For the maximum performance of Fe_3O_4 adsorbent, the optimal working pH lies between 7.5 and 8.5, which falls within the typical pH range of groundwater (Heath 1984), and therefore makes the material highly promising for that application.

For a better understanding of the pH effects on adsorption, the zeta potential and particle size were measured at several different pH values, ranging from 2 to 12, and the results are presented in Figure 6.

The relationships between the zeta potential and pH are revealed in Figure 6 (a) and a major trend of decrease in zeta potential with increasing pH is observed. When pH is lower than 6, the zeta potential decreases quickly as pH increases, from 22.53 mV at pH=2.26 to -32.3 mV at pH=6.07, and the isoelectric point is found at pH=4.28 by interpolation. At pH higher than 6, the zeta potential decreases slowly to -42.3 mV as pH increases to 11.44. Figure 6 (b) shows the correlations between the particle size of Fe_3O_4 and pH. At lowest pH of 2.26, the particle size was estimated to be 1081 nm. As pH approaches the isoelectric point, the

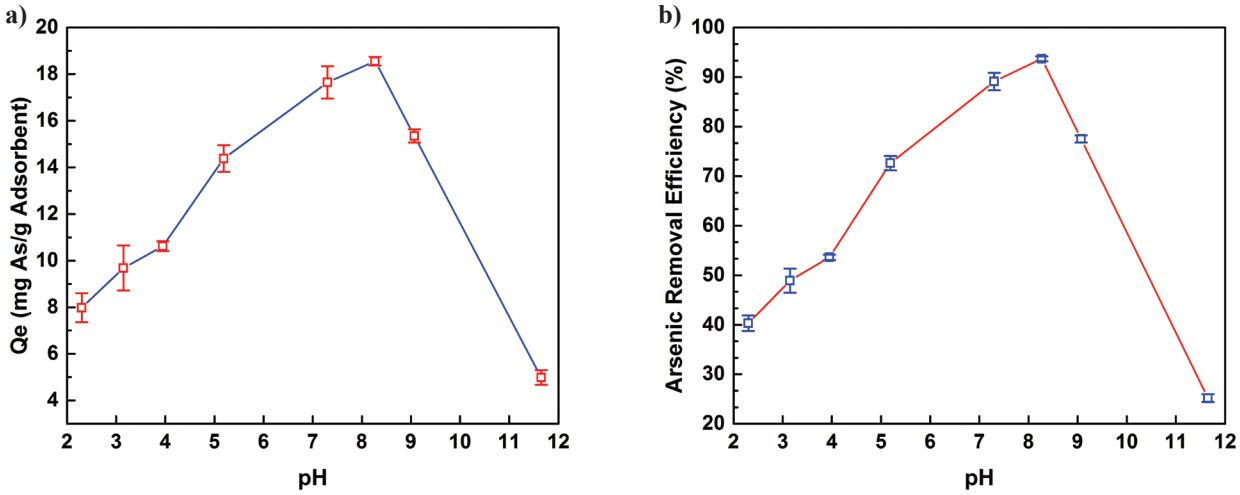

Figure 5. (a) Adsorption capacity of Fe_3O_4 at different pH. (b) Arsenic removal efficiencies at different pH.

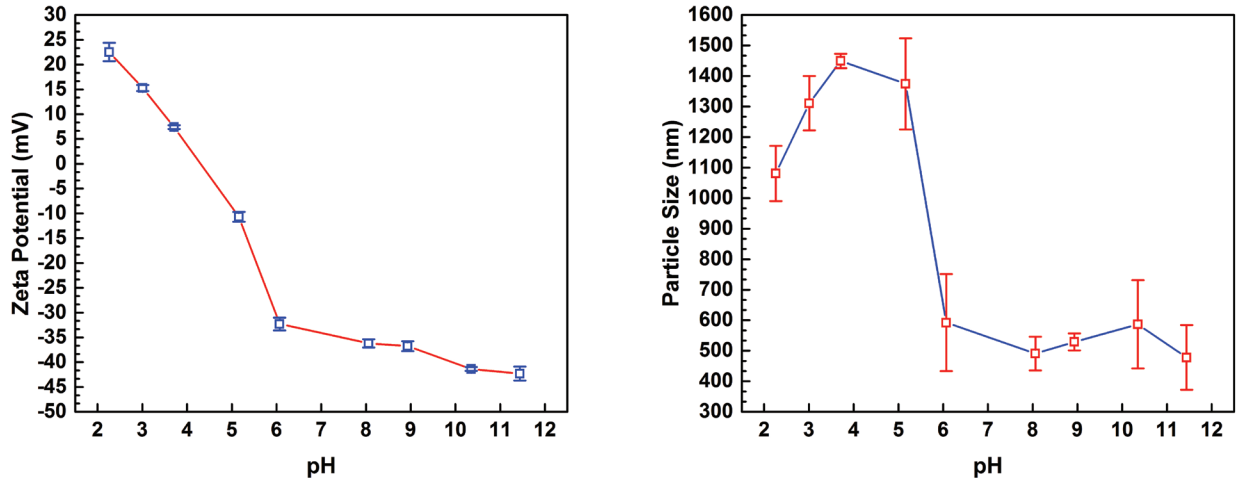

Figure 6. (a) Zeta potential of Fe_3O_4 at different pH. (b) Particle size of Fe_3O_4 in solution at different pH.

particle size gradually increases to 1449.5 nm at pH=3.71, indicating the adsorbent is less dispersed and coagulation would occur. Once above the isoelectric pH, the particle size will decrease with further increase in pH. It should be noted that the particle size decreased significantly from 1374.5 nm to 592.07 nm as pH changed from 5.16 to 6.07, suggesting the dispersion of adsorbent is much better. Meanwhile, for a fixed amount of adsorbent, smaller particle size means more available surface area for adsorption. When pH is elevated from 8.06 to 11.44, the change in the particle size is relatively small (490.75 nm at pH=8.06, 529 nm at pH=8.93, 586.5 nm at pH=10.35, and 478.2 nm at pH=11.44), which is in agreement with the small change in zeta potential.

The pH effects on adsorption could be considered as comprehensive effects of the zeta potential, particle size of the adsorbent, and existing form of As(V). As a triprotic acid, the deprotonation dissociation constants (pK_a) of arsenate are 2.20 ($H_3AsO_4/H_2AsO_4^-$), 6.97 ($H_2AsO_4^-/HAsO_4^{2-}$), and 11.53 ($HAsO_4^{2-}/AsO_4^{3-}$). When pH increases from 2.3 to 3.95, the zeta potential of Fe_3O_4 decreases while $H_2AsO_4^-$, the species with a negative charge, gradually becomes the dominating existing form of arsenate. We conjecture that the transformation of uncharged H_3AsO_4 into negative charged $H_2AsO_4^-$ could overcome the decreases in zeta potential of the adsorbent and the overall adsorption capacity increases. As mentioned previously, a sharp decrease in the particle size is observed when

pH is higher than 5 and the particle size hits its minimum value at pH around 8. In this region, though the zeta potential of Fe_3O_4 is negative and arsenate exists as anions ($H_2AsO_4^-$/$HAsO_4^{2-}$), the significant decrease in particle size provides more surface areas for adsorption and the formation of surface complexation compounds (Cornell and Schwertmann 2003). Therefore, the adsorption capacity increases and reaches its maximum value at pH=8.27. Further increase in pH has little effects on the zeta potential and particle, but arsenate will gradually transform into a more negative charged species, AsO_4^{3-}, leading to higher electrostatic repulsion. Meanwhile, the competition adsorption of OH^- on the surface of Fe_3O_4 was also reported (Cornell and Schwertmann 2003). Consequently, the adsorption capacity of Fe_3O_4 decreases quickly with increasing pH. The fact that significant adsorption of the negatively charged As(V) at pHs where the surface is also negative further indicates that the interaction is specific in nature as initially proposed.

Adsorption Kinetics

The kinetics of As(V) removal by Fe_3O_4 adsorbent was determined with an initial As(V) concentration of 1 ppm (Figure 7 (a)). A sharp decrease in As(V) concentration, from 1000 ppm to 270 ppm, is observed for the first 2.5 minutes and the corresponding As(V) removal efficiency during this period is 73%. Since then, the rate of As(V) is much lower and gradually decreases with time. The adsorption of As(V) on goethite and hematite has also been reported to follow a two stage mechanism, with a fast initial rate followed by a much slower rate (Singh et al. 1988; Grossl et al. 1997; Sabbatini et al. 2010). The adsorption-desorption equilibrium is established after 120 minutes with a residual As(V) concentration of 175 ppb and a removal efficiency of 82.5%. Considering that the adsorbent loading is much lower in kinetics studies than in other experiments (100 mg/L vs. 1000 mg/L), it is believed that fast As(V) removal with better efficiency could be obtained with higher adsorbent loading. For comparison, in the isotherm studies at pH=7.6, the residual As(V) concentration is only 8.02 ppb when initial As(V) concentration is 1 ppm.

Two kinetics models, pseudo-first-order and pseudo-second-order model, were applied to fit experimental data. Pseudo-first-order model is expressed as:

$$\log(Q_e - Q_t) = \log(Q_e) - k_1 t \qquad \text{(Eq. 8)}$$

where Q_e and Q_t represent the mass of As(V) adsorbed per mass of adsorbent (mg/g) at equilibrium and at time t; k_1 is the rate constant of pseudo-first-order model. The logarithm term $\log(Q_e - Q_t)$ is plotted against t in Figure 7 (b) and the correlation coefficient R^2 is 0.8399, thus indicating the adsorption of As(V) by Fe_3O_4 is unlikely to follow the pseudo-first-order model.

Pseudo-second-order model is then used for data fitting and its rate equation in differential form is given as:

$$\frac{dQ_t}{dt} = k_2(Q_e - Q_t)^2 \qquad \text{(Eq. 9)}$$

where k_2 is the rate constant of pseudo-first-order model ($g \cdot mg^{-1} \cdot min^{-1}$). Equation 9 is then linearized by taking integration from t=0 to t=t:

$$\frac{t}{Q_t} = \frac{1}{Q_e} t + \frac{1}{K_2 Q_e^2} \qquad \text{(Eq. 10)}$$

$\frac{t}{Q_t}$ is plotted against t in Figure 7 (c) and the model has a stronger coefficient of determination than the pseudo-first-order model, with an R^2 of 0.9908.The initial adsorption rate r_0 ($mg \cdot g^{-1} \cdot min^{-1}$) is derived from Equation 9 by setting Q_t equal to zero and substituting Q_e and k_2:

$$r_0 = k_2 Q_e^2 \qquad \text{(Eq. 11)}$$

Q_e, k_2, and r_0 are calculated to be 4.30 mg/g, 0.2754 $g \cdot mg^{-1} \cdot min^{-1}$, and 5.0985 $mg \cdot g^{-1} \cdot min^{-1}$, respectively. It should also be noted that Q_e predicted from pseudo-second-order model is in agreement with the adsorption capacity from equilibrium experiments.

Conclusions

In this work, 2D Fe_3O_4 nanosheets were synthesized and their arsenic removal performance was evaluated. XRD analysis of the adsorbent verified the presence of Fe_3O_4 in the bulk phase; peaks for Fe_2O_3 were also observed. The BET specific surface area of the adsorbent was 94.07 m^2/g and 2D structures were confirmed by TEM.

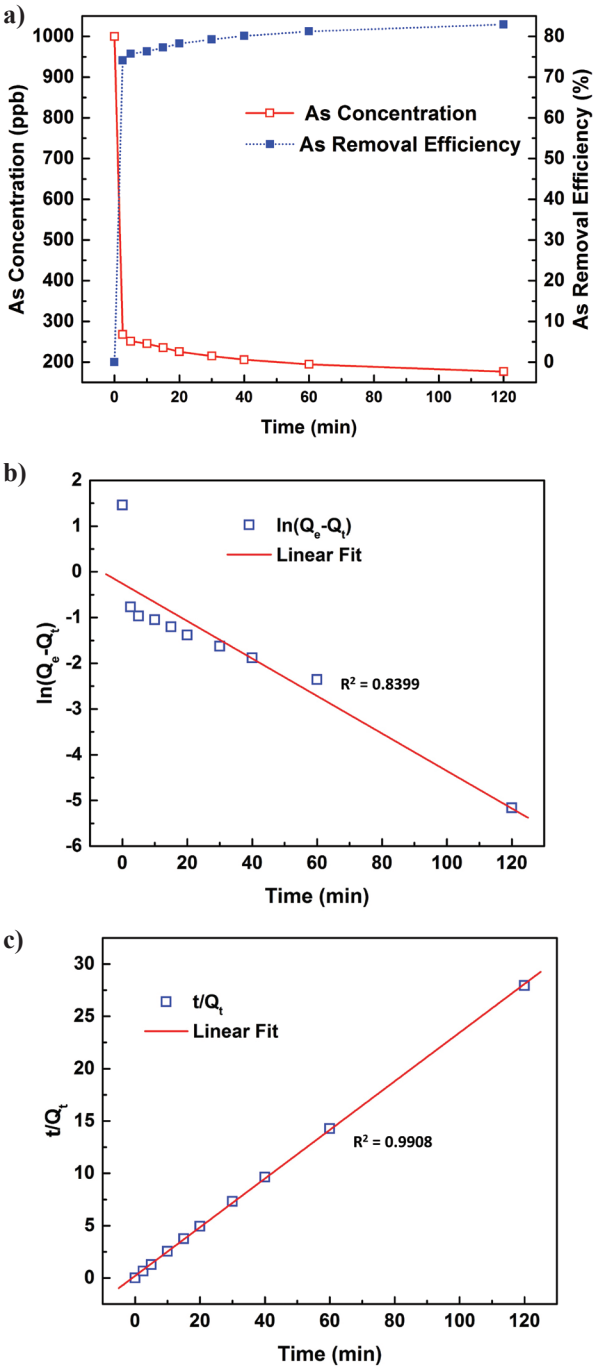

Figure 7. (a) Kinetic adsorption data for As(V) by Fe_3O_4 adsorbent. Data fitting with (b) pseudo-first-order kinetic model and (c) pseudo-second-order kinetic model.

Isotherm studies at both pH=4.7 and 7.6 proved that the adsorption behaviors of As(V) onto Fe_3O_4 adsorbent were better described by the Freundlich isotherm model. Corresponding parameters K_f and $1/n$ were 6.5562 mg/g and 0.4609 at pH=4.7 and 11.194 mg/g and 0.5376 at pH=7.6, respectively. The effect of pH was studied and the optimal value was found at 8.27, where the adsorption capacity and the removal efficiency were 18.55 mg/g and 93.69%. Further investigation suggested that the pH dependence was the result of the influence of the zeta potential, particle size of the adsorbent, and existing form of As(V). Kinetics studies showed that the As(V) adsorption by Fe_3O_4 adsorbent followed the pseudo-second-order model; 73% of the As(V) was adsorbed within the first 2.5 minutes and an overall removal efficiency of 82.5% was achieved in 2 hours of reaction. However, enhanced removal efficiency could be expected at higher adsorbent loading. Therefore, we believe that Fe_3O_4 nanosheets are a competitive adsorbent material for arsenic removal due to their good adsorption capacity, fast kinetics, and easy separation.

Acknowledgments

The manuscript was prepared through contributions of all authors. All authors have approved the final version of the manuscript.

Author Bio and Contact Information

Hongxi Luo received a B.S. in Chemical Engineering (2016) from University of Missouri, where he conducted research under the supervision of Dr. Maria Fidalgo and East China University of Science & Technology. He is currently a graduate student in Chemical Engineering at University of Virginia. His current research interests includes tuning polymer backbone structures for new membrane design and understanding the effects of polymer backbones on ion transport across the membrane. He may be contacted at hldm5@mail.missouri.edu.

Fangwei Cheng holds a B.S. degree in Chemical Engineering (2015) from Wuhan Institute of Technology and a M.S degree in Chemical Engineering (2016) from University of Missouri. She is currently a graduate student in Civil & Environmental Engineering at University of Virginia. Her current research interests include designing new organoclays and improving the efficiency and efficacy of wastewater

treatments for removal of certain organic contaminants. She may be contacted at fcnp3@mail.missouri.edu.

Weiming Hu is a Ph.D. candidate in Department of Civil & Environmental Engineering at University of Missouri – Columbia. His research interests include water/wastewater treatment processes, adsorption process, and materials science in environmental applications. He may be contacted at why78@mail.missouri.edu.

Jinpeng Wang received a B.S. degree in Chemical Engineering from University of Missouri (2015) and a Master of Engineering (MEng) degree in Chemical Engineering & Applied Chemistry from University of Toronto in Feb 2017. His current research interests are focused on Ultraviolet (UV) light reactors for drinking water treatment. He may be contacted at jinpeng.wang@mail.utoronto.ca.

Shuting Xiang received her B.S. degree in Chemical Engineering from University of Missouri (2017). She joined Dr. Maria Fidalgo's group from September 2015. Her current research interests are focused on fabrication and characterization of highly porous films, designed for the capture of pollutants in water. She may be contacted at sx6cf@mail.missouri.edu.

Maria Fidalgo is an Associate Professor in the Department of Civil and Environmental Engineering at the University of Missouri. She holds a B.S. in Chemical Engineering from Instituto Tecnologico de Buenos Aires, Argentina, and M.S. and Ph.D. degrees in Environmental Engineering from Rice University. Her area of interest includes the interactions of nanomaterials and natural systems, physicochemical processes (membrane separations and advanced oxidation) and nano-enabled environmental sensors. She may be contacted at fidalgom@missouri.edu.

References

Ajay, K., M. Agrawal, P. Chandrashekhar, L. Ishwardas, and L. Muthreja. 2014. Langmuir, Freundlich and BET adsoprtion isotherm studies for zinc ions onto coal fly ash. *International Journal of Application or Innovation in Engineering Management* 3(1): 7.

Amano, Y., Y. Matsushita, and M. Machida. 2014. Arsenic adsorption by activated carbon with different amounts of basic sites under different solution pH and coexistent ions. *Separation Science and Technology* 49(3): 345-353.

Anderson, P. and D. Malotky. 1979. The adsorption of protolyzable anions on hydrous oxides at the isoelectric pH. *Journal of Colloid Interface Science* 72: 15.

Borys, P. and Z. Grzywna. 2016. On the fractality of the Freundlich adsorption isotherm in equilibrium and non-equilibrium cases. *Physical Chemistry Chemical Physics* 18(30): 20784-20789.

Chang, S., Y. Yu, C. Li, C. Wu, and H.-Y. Lei. 2012. Highly efficient arsenic removal using a composite of ultrafine magnetite nanoparticles interlinked by silane coupling agents. *International Journal of Environmental Research & Public Health* 9(10): 3711-3723.

Cheng, F., H. Luo, L. Hu, B. Yu, Z. Luo, and M. Fidalgo de Cortalezzi. 2016. Sludge carbonization and activation: From hazardous waste to functional materials for water treatment. *Journal of Environmental Chemical Engineering* 4(4A): 4574-4586.

Cornell, R. and U. Schwertmann. 2003. *The Iron Oxides: Structure, Properties, Reactions, Occurences and Uses, 2nd edition*. WILEY-VCH Verl. GmbH Co KGaAWeinheim.

Dixit, S. and J. Hering. 2003. Comparison of arsenic(V) and arsenic(III) sorption onto iron oxide minerals: Implications for arsenic mobility. *Environmental Science & Technology* 37(18): 4182-4189.

Fan, T., D. Pan, and H. Zhang. 2011. Study on formation mechanism by monitoring the morphology and structure evolution of nearly monodispersed Fe_3O_4 submicroparticles with controlled particle sizes. *Industrial & Engineering Chemistry Research* 50(15): 9009-9018.

Giles, D., M. Mohapatra, T. Issa, S. Anand, and P. Singh. 2011. Iron and aluminium based adsorption strategies for removing arsenic from water. *Journal of Environmental Management* 92(12): 3011-3022.

Grossl, P., M. Eick, D.L. Sparks, S. Goldberg, and C.C. Ainsworth. 1997. Arsenate and chromate retention mechanism on goethite. 2: Kinetic evaluation using a pressure-jump relaxation technique. *Environmental Science & Technology* 31: 6.

Guan, X., T. Su, and J. Wang. 2009. Quantifying effects of pH and surface loading on arsenic adsorption on NanoActive alumina using a speciation-based model. *Journal of Hazard Materials* 166(1): 39-45.

He, Z., C.-Y. Xu, L. Zhen, and W.-Z. Shao. 2007. Hydrothermal synthesis and characterization of single crystalline Fe3O4 nanowires with high aspect ratio and uniformity. *Materials Lett*ers 61(14-15): 3159-3162.

Heath, R.C. 1984. *Ground-water Regions of the United States.* Report 2242.

Hingston, F., A. Posner, and J. Quirk. 1968. Adsorption of selenite by goethite. *Advances in Chemistry Series* 79: 9.

Hingston, F., A. Posner, and J. Quirk. 1971. Competitive adsorption of negatively charged ligands on oxide surfaces. *Discussions of the Faraday Society* 52: 9.

Hughes, M.F. 2002. Arsenic toxicity and potential mechanisms of action. *Toxicology Letters* 133(1): 1-16.

Hung, D., O. Nekrassova, and R. Compton. 2004. Analytical methods for inorganic arsenic in water: A review. *Talanta* 64(2): 269-277.

Jain, C. and R. Singh. 2012. Technological options for the removal of arsenic with special reference to South East Asia. *Journal of Environmental Management* 107: 1-18.

Litter, M., M. Morgada, and J. Bundschuh. 2010. Possible treatments for arsenic removal in Latin American waters for human consumption. *Environmental Pollution* 158(5): 1105-1118.

Lumsdon, D., A. Fraser, J. Russell, and N. Livesey. 1984. New infrared band assignments for the arsenate ion adsorbed on synthetic goethite (a-FeOOH). *Journal of Soil Science* 35: 6.

Manceau, A. 1995. The mechanism of anion adsorption on iron oxides. Evidence for the bonding of arsenate tetrahedra at free Fe(O, OH) edges. *Geochimica et Cosmochimica Acta* 59: 7.

Mandal, B. and K. Suzuki. 2002. Arsenic round the world: A review. *Talanta* 58(1): 201-235.

Manning, B. and S. Fendorf. 1998. Surface structures and stability of arsenic(III) on goethite: Spectroscopic evidence for inner-sphere complexes. *Environmental Science & Technology* 34: 6.

Mohan, D. and C. Pittman. 2007. Arsenic removal from water/wastewater using adsorbents--A critical review. *Journal of Hazard Materials* 142(1-2): 1-53.

O'Reilly, S., D. Strawn, and D.L. Sparks. 2001. Residence time effects on arsenate adsorption/ desorption mechanisms on goethite. *Soil Science Society of America Journal* 65: 2.

Pierce, M. and C. Moore. 1980. Adsorption of arsenite on amorphous iron hydroxide from dilute aqueous solution. *Environmental Science & Technology* 14: 3.

Pierce, M. and C. Moore. 1982. Adsorption of arsenite and arsenate on amorphous iron hydroxide. *Water Research* 16: 7.

Sabbatini, P., F. Yrazu, F. Rossi, G. Thern, A. Marajovsky, and M. Fidalgo de Cortalezzi. 2010. Fabrication and characterization of iron oxide ceramic membranes for arsenic removal. *Water Research* 44: 11.

Shipley, H., S. Yean, A. Kan, and M. Tomson. 2009. Adsorption of arsenic to magnetite nanoparticles: Effect of particle concentration, pH, ionic strength, and temperature. *Environmental Toxicology Chem*istry 28(3): 509-515.

Singh, D., G. Prasad, D. Rupainwar, and V. Singh. 1988. As(III) removal from aqueous solution by adsorption. *Water, Air, & Soil Pollution* 42: 14.

Smedley, P. and D. Kinniburgh. 2002. A review of the source, behaviour and distribution of arsenic in natural waters. *Applied Geochemistry* 17(5): 517-568.

Styblo, M., L.M. Del Razo, L. Vega, D.R. Germolec, E.L. LeCluyse, G.A. Hamilton, W. Reed, C. Wang, W.R. Cullen, and D.J. Thomas. 2000. Comparative toxicity of trivalent and pentavalent inorganic and methylated arsenicals in rat and human cells. *Archives of Toxicology* 74(6): 289-299.

Sun, J., P. Zan, X. Yang, L. Ye, and L. Zhao. 2016. Room-temperature synthesis of Fe3O4/Fe-carbon nanocomposites with Fe-carbon double conductive network as supercapacitor. *Electrochimica Acta* 215: 483-491.

Sun, X. and H. Doner. 1996. An investigation of arsenate and arsenite bonding structures on goethite by FTIR. *Soil Science* 161: 865-872.

Sun, X. and H. Doner. 1998. Adsorption and oxidation of arsenite on goethite. *Soil Science* 165: 10.

Sun, Z, T. Liao, Y. Dou, S.M. Hwang, M. Park, L. Jiang, J.H. Kim, and S.X. Dou. 2014. Generalized self-assembly of scalable two-dimensional transition metal oxide nanosheets. *Nature Communications* 5: 3813.

Waychunas, G., B. Rea, C. Fuller, and J. Davis. 1993. Surface chemistry of ferrihydrite: Part 1. EXAFS studies of the geometry of coprecipitated and adsorbed arsenate. *Geochimica et Cosmochimica Acta* 57: 19.

Xu, G., L. Li, Z. Shen, Z. Tao, Y. Zhang, H. Tian, X. Wei, G. Shen, and G. Han. 2015. Magnetite Fe3O4 nanoparticles and hematite α-Fe2O3 uniform oblique hexagonal microdisks, drum-like particles and spindles and their magnetic properties. *Journal of Alloys & Compounds* 629: 36-42.

Yavuz, C, J.T. Mayo, W.W. Yu, A. Prakash, J.C. Falkner, S. Yean, L. Cong, H.J. Shipley, A. Kan, M. Tomson, D. Natelson, and V.L. Colvin. 2006. Low-field magnetic separation of monodisperse Fe3O4 nanocrystals. *Science* 314(5801): 964-967.

Yazdani, (Roza) M., T. Tuutijärvi, A. Bhatnagar, and R. Vahala. 2016. Adsorptive removal of arsenic(V) from aqueous phase by feldspars: Kinetics, mechanism, and thermodynamic aspects of adsorption. *Journal of Molecular Liquids* 214: 149-156.